

A functional renormalization group study of the two dimensional Su-Schrieffer-Heeger-Hubbard model

Qing-Geng Yang,¹ Da Wang,^{1,2} and Qiang-Hua Wang^{1,2,*}

¹National Laboratory of Solid State Microstructures & School of Physics, Nanjing University, Nanjing 210093, China

²Collaborative Innovation Center of Advanced Microstructures, Nanjing University, Nanjing 210093, China

We study the Hubbard model on the square lattice coupled in addition to the optical Su-Schrieffer-Heeger (SSH) phonons, using the singular-mode functional renormalization group method. At half-filling and in the absence of the Hubbard interaction U , we find the d-wave Pomeranchuk instability (PI) at weak electron-phonon coupling strength λ , the degenerate spin-density-wave (SDW)/charge-density-wave (CDW)/s-wave superconductivity (sSC) state at larger λ and higher phonon frequency ω , and the valence bond solid (VBS) state at larger λ and lower ω . After switching on a positive U , the PI and VBS states are suppressed, while the SDW state is enhanced. At finite doping, the SSH phonon is found to favor sSC at $U = 0$. With increasing positive U , we find d-wave superconductivity (dSC) and incommensurate SDW states. In a narrow window of moderate U and λ , we also find the incommensurate VBS state. The sSC and dSC here can be naturally related to the CDW and SDW fluctuations, both of which can be triggered by the SSH phonons. In contrast, the repulsive interaction U enhances SDW but suppresses CDW fluctuations. Our results at half filling are consistent with quantum Monte Carlo (QMC) together with the new nematic state, and provide new insights at finite doping where QMC may suffer from the minus sign problem.

I. INTRODUCTION

Electron-phonon interaction (EPI) is one of the fundamental interactions in condensed matter physics. It plays important roles in many quantum phenomena, such as Peierls transition¹, topological solitons², and Bardeen-Cooper-Schrieffer (BCS) superconductivity³. Over the past few decades, a growing number of experiments suggest that the EPI may be necessary in understanding various novel phenomena in strongly correlated materials^{4–16}, which has stimulated many theoretical studies in this direction^{17–31}. Among different types of EPIs, the Su-Schrieffer-Heeger (SSH) model was first introduced to study the physics of *trans* polyacetylene^{2,32}. Interestingly, the original acoustic SSH phonon model is found to give similar results to the optical SSH phonon model^{33,34} since the dominant scattering process mainly involve the phonon modes near zone boundary rather than zone center. In the new century, the SSH model gets renewed attention as it can be taken as the simplest one dimensional (1D) topological insulator³⁵, can be mapped to a 1D topological superconductor³⁶, and has been realized in optical lattices^{37–39}.

Recently, the studies of the 1D SSH model have been extended to two dimensions (2D)^{40–46}. The optical SSH model on the square lattice without or with the Hubbard interaction U has been carefully studied by the quantum Monte Carlo (QMC) method at half filling, where the negative sign problem is absent. In the anti-adiabatic limit (with the phonon frequency $\omega \rightarrow \infty$), the EPI induces effectively an instantaneous bond-wise interaction and has been studied in an early work⁴⁰. In the absence of U , it is found that a degenerate spin-density-wave (SDW)/charge-density-wave (CDW)/s-wave superconductivity (sSC) state is present for any nonzero EPI strength. Both the CDW and SDW states have momen-

tum $\mathbf{Q} = (\pi, \pi)$, while the sSC is at momentum zero (or uniform). The degeneracy is protected by the underlying spin-SU(2), charge-SU(2), and a Z_2 symmetry that transforms between the two sectors.⁴⁷ A spontaneous symmetry breaking in the internal space is needed for the system to settle down in a specific one of the degenerate states. After a repulsive U is turned on, the Z_2 symmetry is broken and the SDW state is the only instability in the anti-adiabatic limit.⁴⁰

For finite phonon frequency and $U = 0$, the degenerate SDW/CDW/sSC order still exist for weak EPI, but a strong enough EPI drives the system into a charge-bond-order (CBO) state with ordering momentum $\mathbf{Q} = (\pi, \pi)$, which is also referred to as valence-bond-solid (VBS) or bond-order-wave in some literature^{41,42}. In fact, this can also be regarded as a generalized CDW state for charges defined on bonds rather than on sites. For comparison, in one-dimensional (1D) SSH model, any nonzero EPI can induce the CBO, referred to as dimerization,^{33,48,49} as a result of the Peierls instability¹. The effect of a finite Hubbard U has also been considered very recently^{43–46}. Since U breaks the Z_2 symmetry, a positive U enhances the SDW in the spin channel while suppresses the CDW/sSC in the charge channel, providing a new avenue to explore the transition between SDW and VBS^{44,50}.

These recent studies uncover rich physics of the 2D SSH-Hubbard model. But most of these studies are restricted to half-filling due to the negative sign problem in QMC at finite doping (and for positive U). In this work, we investigate the optical SSH-Hubbard model with the singular-mode functional renormalization group (SMFRG) method^{51–53} which treats all electronic orders on an equal footing for all cases of interactions and doping levels under concern. At half-filling, we obtain phase diagrams consistent with QMC, except for a nematic Pomeranchuk instability in the weak coupling limit, which has not yet been examined in the literature. Next, we study

the doped case (e.g., with $\langle n \rangle = 0.85$ electrons per site). The SSH phonon always induces sSC in the absence of U , and this can be traced back to the CDW fluctuations the EPI triggers. With increasing positive U , the d-wave SC (dSC) and incommensurate SDW states appear successively. The dSC can be traced back to the antiferromagnetic SDW fluctuations. We also find incommensurate VBS state in a narrow window of moderate U and λ .

The rest of this paper is organized as follows. We describe the model and the SMFRG in Sec. II. Then we present and discuss the results in Sec. III, followed by a summary of this work in Sec. IV.

II. MODEL AND METHOD

We study the SSH-Hubbard model on the square lattice described by the Hamiltonian

$$\begin{aligned}
H = & -t \sum_{\langle ij \rangle \sigma} (c_{i\sigma}^\dagger c_{j\sigma} + \text{H.c.}) - \mu \sum_i n_i + \frac{U}{2} \sum_i (n_i - 1)^2 \\
& + \frac{g}{\sqrt{2M\omega}} \sum_{\langle ij \rangle \sigma} (b_{ij} + b_{ij}^\dagger) (c_{i\sigma}^\dagger c_{j\sigma} + \text{H.c.}) \\
& + \omega \sum_{\langle ij \rangle} \left(b_{ij}^\dagger b_{ij} + \frac{1}{2} \right), \tag{1}
\end{aligned}$$

where t is the hopping integral on nearest neighbor bond $\langle ij \rangle$, $c_{i\sigma}^\dagger$ creates an electron at site i with spin σ , $n_i = \sum_\sigma c_{i\sigma}^\dagger c_{i\sigma}$ is the local electron density, μ is the chemical potential, and U is the on-site Hubbard interaction. We set $t = 1$ as the unit of energy henceforth. The optical SSH phonon is created by b_{ij}^\dagger on each bond $\langle ij \rangle$ with frequency ω . These bond phonons couple to the electrons in the bond charge channel through the g -term, where M denotes the effective mass for the optical vibration.

The model enjoys the natural global spin-SU(2) symmetry. One can also define local pseudo-spins $\vec{\eta}_i = P \vec{S}_i P$, where P is a Nambu transformation such that $P c_{i\uparrow} P = c_{i\uparrow}$, $P c_{i\downarrow} P = (-1)^i c_{i\downarrow}^\dagger$. Explicitly,

$$\eta_j^x = \frac{1}{2} (-1)^j (c_{j\uparrow}^\dagger c_{j\downarrow}^\dagger + c_{j\downarrow} c_{j\uparrow}), \tag{2}$$

$$\eta_j^y = \frac{1}{2} (-1)^j i (c_{j\uparrow}^\dagger c_{j\downarrow}^\dagger - c_{j\downarrow} c_{j\uparrow}), \tag{3}$$

$$\eta_j^z = \frac{1}{2} (n_j - 1). \tag{4}$$

The three components express the local charge, or the deviation from half filling, in different manners. On the other hand, the Hubbard term in H can be rewritten as

$$H_U = \frac{U}{3} \sum_i (\eta_i^2 - \vec{S}_i^2), \tag{5}$$

which changes sign upon the Nambu transformation. At half filling ($\mu = 0$), it can be shown that the total pseudo-spin $\sum_i \vec{\eta}_i$ commutes with the hamiltonian H . In this

case, the Hamiltonian also has charge-SU(2) symmetry. So the model is $SU(2) \times SU(2)/Z_2 = SO(4)$ symmetric (Z_2 here is the staggered particle-hole transformation) for finite U ⁴⁷, and $SO(4) \times Z_2 = O(4)$ [Z_2 here is the staggered partial particle-hole transformation connecting two SU(2) sectors] for $U = 0$ ⁴². A repulsive U favors the formation of local spins, or equivalently suppresses local charge deviation from half filling.

After integrating out the phonons, we obtain a retarded electron-electron interaction described by the action ΔS

$$\Delta S = \frac{1}{2} \sum_{\langle ij \rangle} \int d\tau \int d\tau' B_{ij}(\tau) \Pi(\tau - \tau') B_{ij}(\tau'),$$

where $B_{ij}(\tau) = \sum_\sigma [\bar{c}_{i\sigma}(\tau) c_{j\sigma}(\tau) + \text{c.c.}]$, and \bar{c} and c are Grassman fields. The retarded interaction $\Pi(\tau - \tau')$ written in the frequency space is

$$\Pi(\nu) = -\frac{g^2}{M\omega^2} \frac{\omega^2}{\nu^2 + \omega^2}. \tag{6}$$

Here ν is the bosonic Matsubara frequency, and the minus sign indicates attraction. Note that $M\omega^2 = K$ is just the spring constant for the optical phonon mode. As usual, we write $\Pi(0) = -\lambda W$, with $W = 8$ the bare bandwidth, to define the coupling strength, $\lambda = g^2/(KW)$.

Much of the effects of the SSH phonons can be anticipated and understood qualitatively as follows. (i) In the adiabatic limit $\omega \rightarrow 0$, the SSH phonon acts as classical bond-wise bias fields to the electrons, so it can obviously induce ordering of bond-wise operators. Two types of bond operators are particularly favorable. The first is the Pomeranchuk operator, $(\cos k_x - \cos k_y) c_{k\sigma}^\dagger c_{k\sigma}$ in the momentum space, for which the susceptibility (at zero collective momentum) diverges logarithmically because of the van Hove singularity in the normal state density of states. This operator leads to a nematic state breaking rotation symmetry. The second is the doubly degenerate VBS operators, $i \sin k_x c_{k+\mathbf{Q}\sigma}^\dagger c_{k\sigma}$, for which the susceptibility (at momentum \mathbf{Q}) diverges double-logarithmically because of the van Hove singularity as well as the perfect nesting. Naively one would expect the VBS to be more favorable, but the competition actually also relies on the Fermi-surface matching of the form factors in these operators, as well as the strength of EPI. Our simple mean field calculations, valid in this limit, show that the nematic Pomeranchuk state is realized at weak coupling, while the VBS state wins at stronger coupling. (ii) In the anti-adiabatic limit $\omega \rightarrow \infty$, the phonon-induced action ΔS amounts to an instantaneous interaction

$$\Delta H = -\frac{g^2}{2K} \sum_{\langle ij \rangle} B_{ij}^2 = \frac{2g^2}{K} \sum_{\langle ij \rangle} (\vec{S}_i \cdot \vec{S}_j + \vec{\eta}_i \cdot \vec{\eta}_j - \frac{1}{4}),$$

where B_{ij} is now understood as a bond operator. Clearly, this interaction favors the bond order, as well as the antiferromagnetic ordering of local spins or local pseudo-spins. At half filling, the latter orders are related by

the Nambu transformation, so that the antiferromagnetic spin order is degenerate with the uniform s-wave pairing and CDW at momentum \mathbf{Q} . Since the form factor for the local spin is unity, and the susceptibility diverges double-logarithmically, the local spin ordering, up to the O(4)-symmetry, may be more favorable in the anti-adiabatic limit. One then anticipates a transition from bond-wise order at low phonon frequency to site-local order at high frequency. (iii) On the other hand, from the expression of H_U , it is clear that a repulsive U favors (suppresses) the ordering in the site-local spin (charge) channel. (iv) Away from half filling, the charge-SU(2) symmetry is broken, and both the van Hove singularity and perfect nesting are absent. We then expect weakening of orderings in the particle-hole channels, while the pairing susceptibility in the Cooper channel is always logarithmically divergent. We then expect pairing triggered by fluctuations in the CDW and/or SDW channels at weak coupling, and CDW/SDW/VBS at incommensurate momentum at strong coupling.

The plethora of ordering tendencies in the SSH-Hubbard model discussed above must be treated on the same footing. For this purpose, we resort to SMFRG^{51–53}. The idea of FRG is to inspect the flow of one-particle irreducible vertices, namely, the effective interactions between quasiparticles, with respect to a decreasing infrared cutoff energy scale Λ (the smallest Fermion Matsubara frequency in our case). As in usual practice, we limit ourselves to the four-point vertices. It is understood that by power counting this truncation is valid, controlled and self-consistent if the instability occurs at low energy scales. We will therefore limit ourselves to weak and moderate coupling regimes. The effect of EPI is taken into account through $\Pi(\nu)$, which enters the flow equations as described in Ref.¹⁸. The four-point vertex functions can be rewritten (or decomposed) as scattering matrices for all types of fermion bilinears in all collective channels, namely, the pairing channel for SC, the SDW and CDW channels. Since the various decompositions are performed with respect to the same interaction vertices, the ordering tendencies in the three channels are treated on the same footing. In SMFRG, the fermion bilinears are truncated in the internal spatial range between the two fermions within a fermion bilinear, up to a range L_c that is sufficient to capture all types of potential singular scattering modes. Note that the setback distance between two bilinears is unlimited, and the dependence in this distance is resolved by the collective momentum of the bilinear. The SMFRG is strictly momentum conserving, and is asymptotically exact (up to the four-point vertices) at large L_c . In practice, $L_c = \sqrt{2}$ in our case is sufficient to capture all potential orders involving fermion bilinears defined on-site, on nearest-neighbor bonds and on next-nearest-neighbor bonds. This includes the local (as well as nonlocal) spins in the SDW channel; local charges, Pomeranchuk operator and VBS operator in the CDW channel; local s-wave pairing and d-wave pairing on bonds in the SC channel,

etc. The SMFRG has been applied successfully in various contexts^{18,51–60}, and recently it is also re-interpreted as truncated-unity FRG⁶¹. We monitor the leading (largest negative) singular values S of the scattering matrices in the three channels, as functions of the scale Λ (as well as the collective momentum \mathbf{q}). The first divergence of S in one out of the three channels indicates the instability of the normal state toward the formation of a long range order in that channel. The corresponding energy scale Λ_c gives a measure of the transition temperature T_c of that order, and the eigen scattering mode (as well as the associated momentum) describes how fermion bilinears are linearly combined into the order parameter. We refer to the literature^{18,53,59} for more technical details.

III. RESULTS AND DISCUSSIONS

We performed systematic calculations using SMFRG to obtain the phase diagrams in Figs.1. For $\langle n \rangle = 1$ and $U = 0$ in Fig.1(a), we find the nematic Pomeranchuk state and the degenerate SDW/CDW/sSC state with increasing λ . The VBS state appears at larger λ and smaller phonon frequency. For $\langle n \rangle = 1$ and $\omega = 0.1t$ in Fig.1(b), we find SDW state for larger U and VBS state for larger λ . For $\langle n \rangle = 0.85$ and $U = 0$ in Fig.1(c), the only instability is sSC for all nonzero phonon frequency and coupling λ . For $\langle n \rangle = 0.85$ and $\omega = 0.1t$ in Fig.1(d), we obtain the sSC, dSC and incommensurate SDW as U increases for a small up to moderate λ . As λ is also large, we find a small window of incommensurate VBS. In the following we substantiate and discuss the details of the FRG flow at typical points in each of the phase diagrams.

A. $\langle n \rangle = 1$ and $U = 0$

Fig. 2(a) shows the FRG flow of the leading singular values S in the three channels for $\omega = \infty$ and $\lambda = 0.005$. Here, a log-log plot is adopted for clarity. At high energy scales, the three channels are degenerate, corresponding to the degenerate SDW/CDW/sSC state. But as Λ decreases, the leading eigen mode in the CDW channel changes from on-site bilinear at collective momentum $\mathbf{q} = \mathbf{Q} = (\pi, \pi)$, to d-wave bilinear on-bond with $\mathbf{q} = 0$. The latter mode then grows up quickly and diverges first. This is the Pomeranchuk instability, which is just a nematic modulation of the hopping integrals along x and y directions, as shown in the inset in Fig. 2(a), where the red (blue) bond indicates strong (weak) hopping. The order parameter for such a state is described by the fermion bilinear $(\cos k_x - \cos k_y)c_{k\sigma}^\dagger c_{k\sigma}$ in momentum space. In this state, the Fermi surface is changed such that the van Hove singularity (VHS) points at $(\pi, 0)$ and $(0, \pi)$ are avoided. The weak coupling limit has not been examined in previous QMC, and it should be interesting to do so in future QMC. However, we remark that the

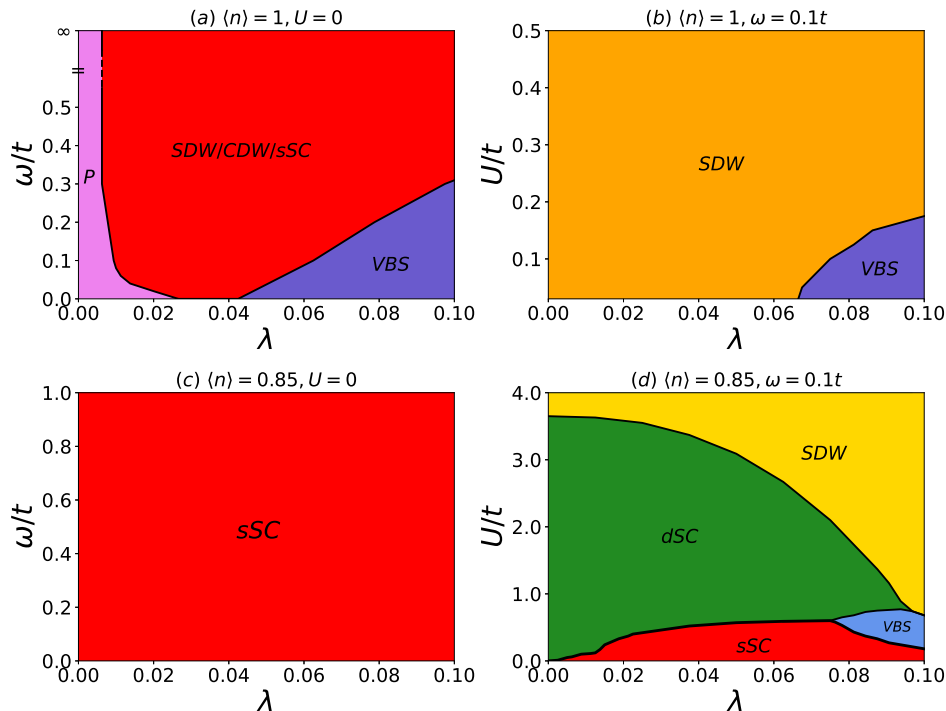


FIG. 1. Phase diagram in the respective parameter space for (a) $\langle n \rangle = 1$ and $U = 0$, (b) $\langle n \rangle = 1$ and $\omega = 0.1t$, (c) $\langle n \rangle = 0.85$ and $U = 0$, and (d) $\langle n \rangle = 0.85$ and $\omega = 0.1t$. Here P denotes the Pomeranchuk state. The other states are defined in the text. The momentum of the SDW/CDW/VBS states is \mathbf{Q} at half filling, and is close to \mathbf{Q} (slightly incommensurate) in the doped case.

order parameter may be weak in this limit, and a large projection time may be needed in QMC to pin down this state.

Fig. 2(b) shows the FRG flow for $\omega = 0.3t$ and $\lambda = 0.025$. At high energy scales, the SC and SDW channels are degenerate, but are split from the CDW channel. This is because the leading scattering mode in the CDW channel is on-bond at high Λ and thus is naturally different to the on-site modes of SDW/sSC at this stage. As the flow continues toward lower energy scales, the three channels merge and diverge simultaneously. We checked that here the leading eigen scattering modes are all local bilinears. The inset shows $S(\mathbf{q})$ in the SC channel as a function of the momentum \mathbf{q} , from which the strong negative peak at $\mathbf{q} = 0$ indicates the Cooper pairing at zero center-of-mass momentum. Meanwhile, the other two channels are found (not shown) to peak at $\mathbf{q} = \mathbf{Q}$, corresponding to the site-local SDW and CDW orders. The existence of such a degenerate SDW/CDW/sSC state is due to the underlying $O(4)$ symmetry, and is consistent with recent QMC results^{40–44}.

In Fig. 2(c), we plot the FRG flow for $\omega = 0.1t$ and $\lambda = 0.075$. During the entire flow, the leading channel is CDW, although the other two channels also catch up quickly at low energy scales, indicating the SSH EPI favors both on-bond VBS and on-site SDW/CDW/sSC orders, and the VBS only wins narrowly. Here, for the VBS, the ordering momentum \mathbf{q} is found to be \mathbf{Q} from

the negative peak in $S(\mathbf{q})$ shown as the lower inset of Fig. 2(c). We find two degenerate scattering modes at this momentum in the CDW channel, $i \sin k_{x,y} c_{k+Q}^\dagger c_k$ in momentum space. The form factor has the p_x or p_y symmetry, and the degeneracy is protected by the little group at \mathbf{Q} (which is the same as the point group). The real-space pattern of this state, up to the two-fold symmetry, is schematically shown in the upper inset of Fig. 2(c), where red/blue color stands for strong/weak bond. In the ordered state, the two degenerate modes may be linearly recombined to minimize the energy.

Our systematic results for this subsection are summarized in Fig. 1(a). We find three competing phases, namely, the nematic phase from Pomeranchuk instability, the degenerate SDW/CDW/sSC phase, and the VBS phase. Except for the new nematic phase not examined previously, our phase boundary agrees well with the QMC result⁴². We should point out that the SDW/CDW/sSC state in our case is degenerate exactly, as our FRG respects all relevant symmetries exactly. However, a spontaneous symmetry breaking may happen in the ordered state, as claimed in QMC⁴², and may be sensitive to the implementation details of QMC. On the other hand, in the weak coupling limit, we always obtain the nematic Pomeranchuk instability for all phonon frequency ω . This is consistent with mean field calculations at $\omega = 0$. Since the present FRG only addresses the first instability as the energy scale is lowered, it is interesting

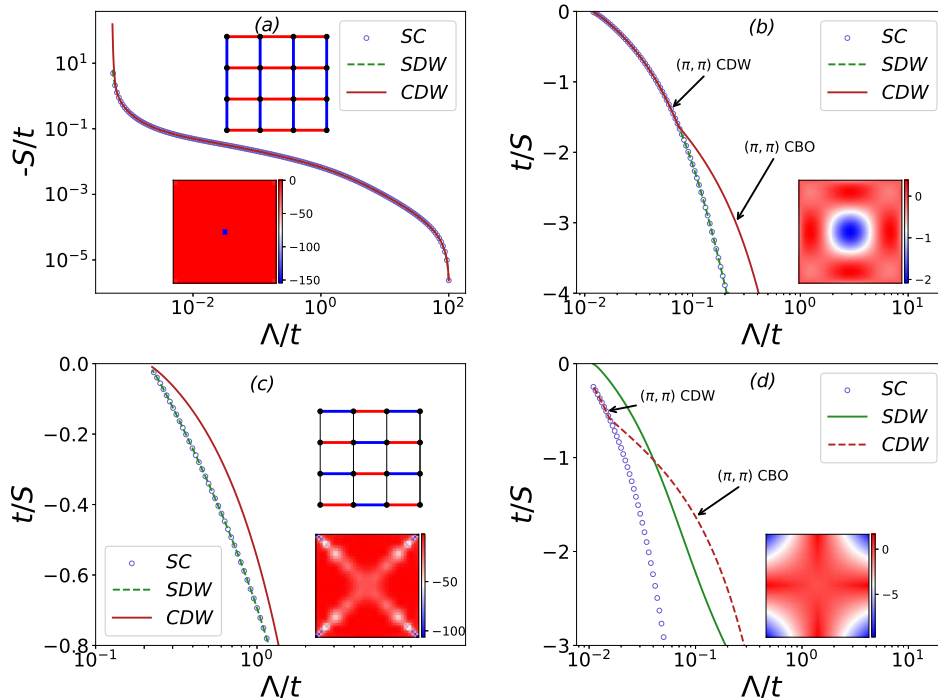


FIG. 2. FRG flows of the leading singular values S in the SC, SDW and CDW channels at half-filling $\langle n \rangle = 1$, in four representative cases: (a) $U = 0$, $\omega = \infty$, and $\lambda = 0.005$. The lower inset shows $S(\mathbf{q})$ in the CDW channel, and the upper inset shows the leading eigen mode, the Pomeranchuk state in real space; (b) $U = 0$, $\omega = 0.3t$, and $\lambda = 0.025$. The inset shows $S(\mathbf{q})$ in the pairing channel. The arrows show there is a level crossing from bond-bilinear to site-bilinear in the CDW channel. At the final stage, the leading eigenvalues in the SDW, CDW, and SC channels are degenerate; (c) $U = 0$, $\omega = 0.1t$, and $\lambda = 0.075$. The lower inset shows $S(\mathbf{q})$ in the CDW channel, and the upper inset shows the leading eigen mode, the VBS state in real space; (d) $U = 0.1t$, $\omega = 0.1t$, and $\lambda = 0.025$. The inset shows $S(\mathbf{q})$ in the SDW channel.

to ask whether the nematic state could develop further instabilities into the SDW/CDW/sSC state, particularly for large phonon frequency.⁶²

B. $\langle n \rangle = 1$ and $U > 0$

The FRG flow for $\omega = 0.1t$, $\lambda = 0.025$ and $U = 0.1t$ is presented in Fig. 2(d). The leading channel at high energy scales is CDW and its scattering mode corresponds to the VBS order, caused by the strong EPI relative to U . As the energy scale is lowered, the SDW channel grows up quickly and diverges first. Its eigen scattering mode is site-local and the collective momentum is \mathbf{Q} from the plot of $S(\mathbf{q})$ (inset) in Fig. 2(d). This is just the antiferromagnetic SDW state. In comparison to the case of $U = 0$ with degenerate SDW/CDW/sSC state, here, a repulsive U breaks the Z_2 symmetry and selects the SDW as the dominant instability. In addition, due to the remaining $SO(4)$ symmetry, the CDW and sSC channels are still degenerate at low energy scales. At high energy scales, the CDW and SC channels split because the leading mode in the CDW channel is not on-site but on-bond. The symmetry only applies to onsite fermion bilinear operators.

For the phonon frequency $\omega = 0.1t$, we obtain the

phase diagram in the (λ, U) space in Fig. 1(b). A large positive U favors SDW, while a large enough λ drives VBS. Since the $O(4)$ symmetry reduces to $SO(4)$ by a finite U , the SDW state has no longer degenerate counterpart in the charge channel. On the other hand, the Pomeranchuk state at $U = 0$ is quickly suppressed for $U > 0.01t$ and is not shown.

C. $\langle n \rangle = 0.85$ and $U = 0$

Next we examine the effect of finite doping. We consider the filling level $\langle n \rangle = 0.85$ as a typical example. The FRG flow for $\omega = 0.1t$ and $\lambda = 0.05$ is shown in Fig. 3(a). At high energy scales, the CDW channel dominates. With decreasing Λ , the SC channel is triggered and eventually diverges first. This behavior indicates the superconductivity is related to charge fluctuations. The leading eigen mode of the SC channel is dominated by onsite electron pair, with center-of-mass momentum $\mathbf{q} = 0$, as seen from the left inset. The right inset shows the pairing function on the Fermi surface. The slight modulation along the Fermi surface comes from the subdominant off-site pairs in the eigen mode.

The phase diagram (for this subsection) in the (λ, ω)

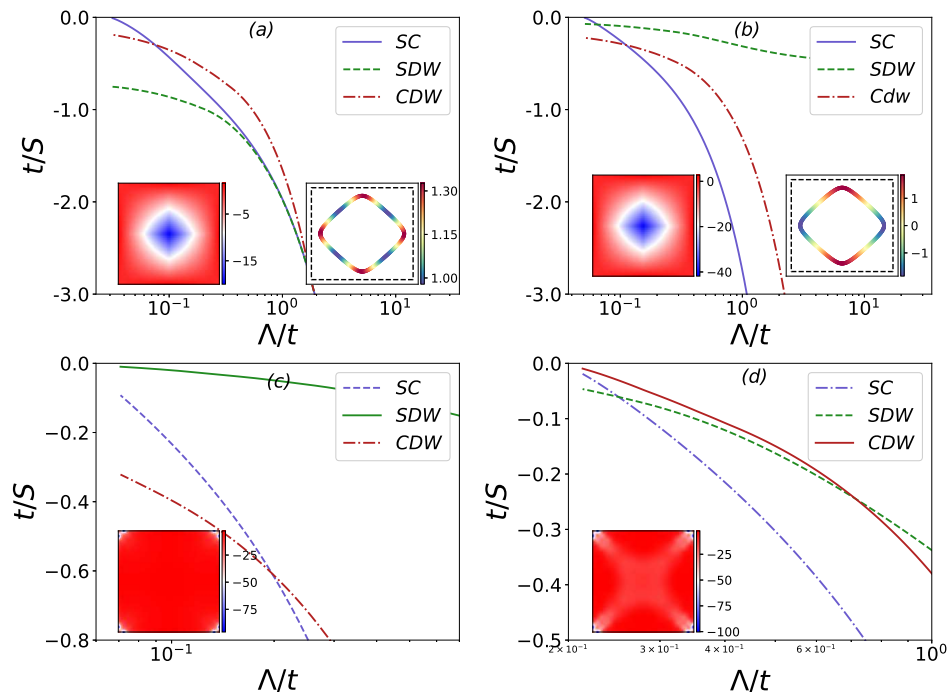


FIG. 3. FRG flows of the leading singular values S in the SC, SDW and CDW channels at doping level $\langle n \rangle = 0.85$, in four representative cases: (a) $U = 0$, $\omega = 0.1t$, and $\lambda = 0.05$. The left inset shows $S(\mathbf{q})$ in the diverging SC channel, and the right inset shows the gap function on the Fermi surface; (b) $U = 2t$, $\omega = 0.1t$, and $\lambda = 0.05$. The insets are defined similarly to that in (a); (c) $U = 3.8t$, $\omega = 0.1t$, and $\lambda = 0.0125$. The inset shows $S(\mathbf{q})$ in the diverging SDW channel; (d) $U = 0.5t$, $\omega = 0.1t$, and $\lambda = 0.0875$. The inset shows $S(\mathbf{q})$ in the diverging CDW channel.

space is shown in Fig. 1(c), with the sSC phase alone up to $\lambda = 0.1$. This is reasonable, since the bare Cooper pairing susceptibility (at $\mathbf{q} = 0$) always enjoys logarithmic divergence as long as the normal state is time-reversal invariant and/or inversion symmetric. Instead, in the particle-hole channels, the divergence is lost once the Fermi surface nesting and van Hove singularity at zero energy are absent upon finite doping.

D. $\langle n \rangle = 0.85$ and $U > 0$

The FRG flow for $\omega = 0.1t$, $\lambda = 0.05$ and $U = 2t$ is shown in Fig. 3(b). At high energy scales, the leading channel is SDW, suggesting strong spin fluctuations caused by Hubbard U . With decreasing Λ , the SC channel is triggered and diverges. The pairing eigen mode is at momentum $\mathbf{q} = 0$ as seen from $S(\mathbf{q})$ in the left inset of Fig. 3(b). The right inset plots the pairing function evaluated on the Fermi surface, which clearly shows the d-wave symmetry. Therefore the system develops dSC, which can be related to the spin fluctuations.

The FRG flow for $\omega = 0.1t$, $\lambda = 0.0125$ and $U = 3.8t$ is shown in Fig. 3(c). During the entire flow, the SDW channel is the leading one. The scattering mode is found to be local, and the collective momentum \mathbf{Q}_1 is incommensurate and near \mathbf{Q} , as can be seen from $S(\mathbf{q})$ in the inset of Fig. 3(c). The incommensurate ordering

momentum is caused by the lacking of perfect nesting at finite doping.

The FRG flow for $\omega = 0.1t$, $\lambda = 0.0875$ and $U = 0.5t$ is presented in Fig. 3(d). Starting from higher energy scale, the SDW and CDW channels are stronger than the SC channel, and the CDW channel grows faster at low energy scales and diverges first. The eigen mode is found to be a bond-wise order similar to the VBS at half filling, except that the ordering momentum \mathbf{Q}_1 is incommensurate and near \mathbf{Q} , see the inset for $S(\mathbf{q})$ in Fig. 3(d). Note that at low energy scales, the SC channel also becomes strong, as a result of the channel overlaps in the various channels.

By systematic calculations, we obtain the phase diagram, Fig. 1(d), for $\langle n \rangle = 0.85$ and $\omega = 0.1t$. For very small $U \ll \lambda W$, the ground state is always sSC. However, this sSC state is suppressed quickly as U increases, and yields to the dSC state and subsequently the incommensurate SDW state for smaller λ . On the other hand, we find the incommensurate VBS state in a narrow window centered at $\lambda \sim 0.09$ and $U \sim 0.5$. The reason that U can tune the balance between the sSC and dSC is because the SSH phonons can trigger both CDW and SDW fluctuations, while a repulsive U enhances (suppresses) the SDW (CDW) fluctuations. The CDW fluctuations are related to sSC, while the SDW fluctuations are related to dSC (in the present model).

IV. SUMMARY

In this work, we have studied the 2D SSH-Hubbard model on the square lattice within SMFRG. The interplay of Hubbard U , EPI strength λ and phonon frequency ω leads to rich phase diagrams. (i) At half-filling and $U = 0$, we obtain degenerate SDW/CDW/sSC state at higher phonon frequency and VBS state at lower frequency and larger λ , in agreement with QMC. At weak coupling, we obtain the interesting nematic state, or the Pomeranchuk state, which is not yet accessed by QMC. A finite U enhances SDW and suppresses the CDW and VBS. (ii) Upon finite doping, we find the sSC alone for

$U = 0$, while an increasing U drives the system into the dSC and incommensurate SDW successively. Besides, the incommensurate VBS state is realized in a narrow window of moderate λ and U . These results at finite doping are beyond the present reach of QMC because of the minus sign problem.

ACKNOWLEDGMENTS

D.W. thanks Z.-X. Liu for helpful discussions on the symmetries. This work is supported by National Natural Science Foundation of China (under Grant Nos. 11874205 and 11574134).

-
- * qhwang@nju.edu.cn
- ¹ R. Peierls, *More Surprises in Theoretical Physics* (Princeton University Press, 1991).
 - ² W. Su, J. Schrieffer, and A. J. Heeger, *Phys. Rev. Lett.* **42**, 1698 (1979).
 - ³ J. Bardeen, L. N. Cooper, and J. R. Schrieffer, *Phys. Rev.* **108**, 1175 (1957).
 - ⁴ A. Lanzara, P. Bogdanov, X. Zhou, S. Kellar, D. Feng, E. Lu, T. Yoshida, H. Eisaki, A. Fujimori, K. Kishio, *et al.*, *Nature* **412**, 510 (2001).
 - ⁵ T. Cuk, D. Lu, X. Zhou, Z.-X. Shen, T. Devereaux, and N. Nagaosa, *Phys. Status Solidi B* **242**, 11 (2005).
 - ⁶ D. Lu, I. M. Vishik, M. Yi, Y. Chen, R. G. Moore, and Z.-X. Shen, *Annu. Rev. Condens. Matter Phys.* **3**, 129 (2012).
 - ⁷ Z. Chen, Y. Wang, S. N. Rebec, T. Jia, M. Hashimoto, D. Lu, B. Moritz, R. G. Moore, T. P. Devereaux, and Z.-X. Shen, *Science* **373**, 1235 (2021).
 - ⁸ Q.-Y. Wang, Z. Li, W.-H. Zhang, Z.-C. Zhang, J.-S. Zhang, W. Li, H. Ding, Y.-B. Ou, P. Deng, K. Chang, *et al.*, *Chin. Phys. Lett.* **29**, 037402 (2012).
 - ⁹ Y. Zhong, Y. Wang, S. Han, Y.-F. Lv, W.-L. Wang, D. Zhang, H. Ding, Y.-M. Zhang, L. Wang, K. He, *et al.*, *Sci. Bull.* **61**, 1239 (2016).
 - ¹⁰ J. Lee, K. Fujita, K. McElroy, J. Slezak, M. Wang, Y. Aiura, H. Bando, M. Ishikado, T. Masui, J.-X. Zhu, *et al.*, *Nature* **442**, 546 (2006).
 - ¹¹ C. Gadermaier, A. Alexandrov, V. Kabanov, P. Kusar, T. Mertelj, X. Yao, C. Manzoni, D. Brida, G. Cerullo, and D. Mihailovic, *Phys. Rev. Lett.* **105**, 257001 (2010).
 - ¹² Q. Song, T. Yu, X. Lou, B. Xie, H. Xu, C. Wen, Q. Yao, S. Zhang, X. Zhu, J. Guo, *et al.*, *Nat. Commun.* **10**, 1 (2019).
 - ¹³ S. Zhang, T. Wei, J. Guan, Q. Zhu, W. Qin, W. Wang, J. Zhang, E. Plummer, X. Zhu, Z. Zhang, *et al.*, *Phys. Rev. Lett.* **122**, 066802 (2019).
 - ¹⁴ W. Zhao, M. Li, C.-Z. Chang, J. Jiang, L. Wu, C. Liu, J. S. Moodera, Y. Zhu, and M. H. Chan, *Sci. Adv.* **4**, eaao2682 (2018).
 - ¹⁵ R. Peng, K. Zou, M. Han, S. D. Albright, H. Hong, C. Lau, H. Xu, Y. Zhu, F. Walker, and C. Ahn, *Sci. Adv.* **6**, eaay4517 (2020).
 - ¹⁶ L. Pintschovius, H. Rietschel, T. Sasaki, H. Mori, S. Tanaka, N. Toyota, M. Lang, and F. Steglich, *EPL (Europhys. Lett.)* **37**, 627 (1997).
 - ¹⁷ A. Mishchenko and N. Nagaosa, *Phys. Rev. Lett.* **93**, 036402 (2004).
 - ¹⁸ D. Wang, W.-S. Wang, and Q.-H. Wang, *Phys. Rev. B* **92**, 195102 (2015).
 - ¹⁹ Y.-H. Liu, R. M. Konik, T. Rice, and F.-C. Zhang, *Nat. Commun.* **7**, 1 (2016).
 - ²⁰ I. Esterlis, B. Nosarzewski, E. W. Huang, B. Moritz, T. P. Devereaux, D. J. Scalapino, and S. A. Kivelson, *Phys. Rev. B* **97**, 140501 (2018).
 - ²¹ N. C. Costa, T. Blommel, W.-T. Chiu, G. Batrouni, and R. Scalettar, *Phys. Rev. Lett.* **120**, 187003 (2018).
 - ²² Z.-X. Li, M. L. Cohen, and D.-H. Lee, *Phys. Rev. B* **100**, 245105 (2019).
 - ²³ Y.-X. Zhang, W.-T. Chiu, N. Costa, G. Batrouni, and R. Scalettar, *Phys. Rev. Lett.* **122**, 077602 (2019).
 - ²⁴ C. Chen, X. Y. Xu, Z. Y. Meng, and M. Hohenadler, *Phys. Rev. Lett.* **122**, 077601 (2019).
 - ²⁵ G. Batrouni and R. T. Scalettar, *Phys. Rev. B* **99**, 035114 (2019).
 - ²⁶ Z. Li, G. Antonius, M. Wu, H. Felipe, and S. G. Louie, *Phys. Rev. Lett.* **122**, 186402 (2019).
 - ²⁷ M. Gao, X.-W. Yan, Z.-Y. Lu, and T. Xiang, *Phys. Rev. B* **101**, 094501 (2020).
 - ²⁸ B. Cohen-Stead, K. Barros, Z. Y. Meng, C. Chen, R. Scalettar, and G. Batrouni, *Phys. Rev. B* **102**, 161108 (2020).
 - ²⁹ C. Feng and R. T. Scalettar, *Phys. Rev. B* **102**, 235152 (2020).
 - ³⁰ J.-Y. Chen, S. A. Kivelson, and X.-Q. Sun, *Phys. Rev. Lett.* **124**, 167601 (2020).
 - ³¹ Y. Wang, Z. Chen, T. Shi, B. Moritz, Z.-X. Shen, and T. P. Devereaux, *Phys. Rev. Lett.* **127**, 197003 (2021).
 - ³² A. J. Heeger, S. Kivelson, J. R. Schrieffer, and W. P. Su, *Rev. Mod. Phys.* **60**, 781 (1988).
 - ³³ E. Fradkin and J. E. Hirsch, *Phys. Rev. B* **27**, 1680 (1983).
 - ³⁴ M. Weber, F. F. Assaad, and M. Hohenadler, *Phys. Rev. B* **91**, 245147 (2015).
 - ³⁵ X.-L. Qi and S.-C. Zhang, *Rev. Mod. Phys.* **83**, 1057 (2011).
 - ³⁶ A. Y. Kitaev, *Physics-Uspekhi* **44**, 131 (2001).
 - ³⁷ M. Atala, M. Aidelsburger, J. T. Barreiro, D. Abanin, T. Kitagawa, E. Demler, and I. Bloch,

- Nature Phys.* **9**, 795 (2013).
- ³⁸ E. J. Meier, F. A. An, and B. Gadway, *Nat. Commun.* **7**, 1 (2016).
- ³⁹ M. Lohse, C. Schweizer, O. Zilberberg, M. Aidelsburger, and I. Bloch, *Nat. Phys.* **12**, 350 (2016).
- ⁴⁰ M. Feldbacher, F. F. Assaad, F. Hebert, and G. G. Batrouni, *Phys. Rev. Lett.* **91**, 056401 (2003).
- ⁴¹ B. Xing, W.-T. Chiu, D. Poletti, R. T. Scalettar, and G. Batrouni, *Phys. Rev. Lett.* **126**, 017601 (2021).
- ⁴² X. Cai, Z.-X. Li, and H. Yao, *Phys. Rev. Lett.* **127**, 247203 (2021).
- ⁴³ X. Cai, Z.-X. Li, and H. Yao, *arXiv preprint arXiv:2112.14744* (2021).
- ⁴⁴ A. Götz, S. Beyl, M. Hohenadler, and F. F. Assaad, *Phys. Rev. B* **105**, 085151 (2022).
- ⁴⁵ C. Feng, B. Xing, D. Poletti, R. Scalettar, and G. Batrouni, “Phase diagram of the su-schrieffer-heeger-hubbard model on a square lattice,” (2022), *arXiv:2109.09206 [cond-mat.str-el]*.
- ⁴⁶ N. K. Yirga, K.-M. Tam, and D. K. Campbell, “Phonon induced instabilities in correlated electron hamiltonians,” (2022), *arXiv:2206.03981 [cond-mat.str-el]*.
- ⁴⁷ C. N. Yang and S. Zhang, *Mod. Phys. Lett. B* **4**, 759 (1990).
- ⁴⁸ P. Sengupta, A. W. Sandvik, and D. K. Campbell, *Phys. Rev. B* **67**, 245103 (2003).
- ⁴⁹ H. Bakrim and C. Bourbonnais, *Phys. Rev. B* **91**, 085114 (2015).
- ⁵⁰ T. Senthil, A. Vishwanath, L. Balents, S. Sachdev, and M. P. A. Fisher, *Science* **303**, 1490 (2004).
- ⁵¹ W.-S. Wang, Y.-Y. Xiang, Q.-H. Wang, F. Wang, F. Yang, and D.-H. Lee, *Phys. Rev. B* **85**, 035414 (2012).
- ⁵² Y.-Y. Xiang, F. Wang, D. Wang, Q.-H. Wang, and D.-H. Lee, *Phys. Rev. B* **86**, 134508 (2012).
- ⁵³ W.-S. Wang, Z.-Z. Li, Y.-Y. Xiang, and Q.-H. Wang, *Phys. Rev. B* **87**, 115135 (2013).
- ⁵⁴ W.-S. Wang, Y. Yang, and Q.-H. Wang, *Phys. Rev. B* **90**, 094514 (2014).
- ⁵⁵ Y. Yang, W.-S. Wang, J.-G. Liu, H. Chen, J.-H. Dai, and Q.-H. Wang, *Phys. Rev. B* **89**, 094518 (2014).
- ⁵⁶ Y.-C. Liu, F.-C. Zhang, T. M. Rice, and Q.-H. Wang, *npj Quantum Materials* **2**, 1 (2017).
- ⁵⁷ Y.-C. Liu, W.-S. Wang, F.-C. Zhang, and Q.-H. Wang, *Phys. Rev. B* **97**, 224522 (2018).
- ⁵⁸ W.-S. Wang, C.-C. Zhang, F.-C. Zhang, and Q.-H. Wang, *Phys. Rev. Lett.* **122**, 027002 (2019).
- ⁵⁹ Q.-K. Tang, L. Yang, D. Wang, F.-C. Zhang, and Q.-H. Wang, *Phys. Rev. B* **99**, 094521 (2019).
- ⁶⁰ Y. Yang, W.-S. Wang, C.-S. Ting, and Q.-H. Wang, *Science Bulletin* **65**, 1901 (2020).
- ⁶¹ J. Lichtenstein, D. Sánchez de la Peña, D. Rohe, E. Di Napoli, C. Honerkamp, and S. Maier, *Computer Physics Communications* **213**, 100 (2017).
- ⁶² C. J. Halboth and W. Metzner, *Phys. Rev. Lett.* **85**, 5162 (2000).